OTC 6760

Offshore Pipelaying: Significance of Motions and Dynamic Stresses During Laying Operations

G.F. Clauss, H. Weede, and A. Saroukh, Technische U. Berlin

This paper was presented at the 23rd Annual OTC in Houston, Texas, May 6–9, 1991.

Abstract

When installing an offshore pipeline, a long pipe span between the vessel and the seabed is exposed to severe static and dynamic loads. A numerical simulation of its dynamic response is developed and experimentally validated. The calculation methods are based on large deflection circular beam theory. The solution is composed of a linear approach in frequency domain and a modally decomposed nonlinear correction in time domain. If the pipe follows the axial motion component of the stinger, a nonlinear interaction between dynamic tension and bending is included. Alternatively, the tensioner may hold the tension force on a constant value, and the resulting relative axial motions between pipe and vessel are determined. Linearized soil reactions are included to simulate the partial absorption of the bending oscillations. Model tests are performed and accompanied by theoretical simulation; the good agreement proves the reliability of the calculation methods. This validation simulates existing full scale prototypes following the special similarity laws of offshore pipelaying. A highly efficient and flexible model testing technique and equipment is used. The significance of dynamic stresses is illustrated by a full scale parameter study.

Introduction

The technique of offshore pipelaying is shown in Fig.1. Segments of steel pipe, weighted and protected by a concrete coating, are connected on board and lowered to the seabed.

In the S-method (Fig. 1), the angle between the horizontal manufacturing position and the steep elastic line is bridged by a circular stinger equipped with rollers. Its curvature radius corresponds at least to the maximum bending stress. To avoid a bending moment peak at the last roller, the pipe must lift off smoothly from the stinger well ahead of its lower end.

In extremly deep water the elastic line becomes so steep that the required stinger length may not be feasible. In this case, the so called J-method is recommended: All welding equipment and the tensioner can be variably inclined to minimize the bending moment at the clamped end.

The effective weight per unit length, as required to fix the pipeline on the seabed, and a possible current yield large static bending stresses, which are limited by pulling the pipe horizontally with the moored vessel. In the seaway, the vessel moves in all degrees of freedom and imposes oscillations to the pipe. Secondarily, the pipe is also loaded by direct wave action near the surface.

A tensioner supports and retains the pipeline on the vessel and supplies the required tension to the unsupported span. The tensioner drive can be operated for partially compensating the dynamic axial loads. This paper discusses both full compensation (no dynamic tension, maximum axial pipe motion relative to the ship) and blocked tensioner (maximum dynamic tension, no axial pipe motion relative to the ship). These two extrema are the boundaries of more sophisticated tensioner driving methods [13] which can be simulated arbitrarily.

Only a few papers on the dynamics of pipelaying have been published up to now.

Early in 1978, Kirk and Etok [11] presented a study of wave induced random vibrations of pipelines suspended in the J-configuration. Their method is based on a linearized spectral analysis. Neither vessel motion nor variation of tension is considered. The pipe ends are assumed as being clamped or hinged.

Malahy [15] developed a general purpose dynamic beam analysis method. It is based on Hamilton's principle applied to a finite element model. An inner loop solves the equation system at each timestep, and an outer loop improves the solution iteratively.

Clauss and Weede [7] published the present method at an earlier stage. As the nonlinear correction in time domain was not yet ready, nonlinearities were simulated by offset effects in the linear frequency domain approach. This "semi-nonlinear" method may still be interesting as a more simple alternative.

The present theoretical analysis is based on large deflection cir-

References and figures at end of paper

cular beam theory clearly summarized as a flowchart-like scheme by Weede [18]. Besides the well known torsional differential equation, it yields the differential equation for the radius vector of the oscillating axis.

Vlahopoulos and Bernitsas [17] are expanding the same vector equation, e.g. for bending rotatory inertia and structural damping. A vector version of Galerkin's method is directly introduced into this equation with a finite element discretization, and a coupled equation system with time dependent matrices is solved with the Newmark method.

As a related topic, riser analysis should be mentioned.

Gardner and Kotch [8] presented the type of dynamic bending equation later used by Hapel and Köhl [9] and in the present paper. They introduced the assumption that the dynamic tension force may be averaged over the length. The present paper transfers this to pipelaying based on [18] and Kirchhoff's hypothesis in [10]. Gardner and Kotch assume that the dynamic tension force is known.

Hapel and Köhl [9] took advantage of the fact that the static tension force in a marine riser increases linearly from bottom to top. After neglecting dynamic tension and flexural rigidity and linearizing the hydrodynamic drag, the dynamic bending equation was solved analytically using modified Bessel functions. Frequency domain analysis performs quite poorly if one evaluates the linearized hydrodynamic damping parameter in time domain. Eq. (18) in this paper is speeded up in practice with an approach presented by Krolikowski and Gay [12]. See also [2].

Cable dynamics differ from the pipelaying problem due to large strain and the absence of flexural rigidity. For the planar case, Bliek and Triantafillou [1] present a linear and a nonlinear solution based on force equilibrium. The nonlinear solution consists of a quasi-stationary part to satisfy the boundary conditions from the vessel's motion and a modally decomposed dynamic part.

Several practical aspects of offshore pipelaying are discussed in [5] and [13].

Based on large deflection beam theory, Clauss et al. [5] published a static analysis of pipelines during laying. Further, a procedure for pipe dimensioning is presented considering the combined stress associated with external pressure and bending moment under laying conditions, allowing for initial out-of-roundness of the pipe.

The most comprehensive variety of practical pipelaying aspects is discussed by Langner and Ayers [13]. This paper covers technical and economical implications of different laying procedures and discusses the question how to operate the tensioner.

Thes present paper presents a unique numerical motion simulation of pipelines during laying. The theoretical analysis of pipe motions and stresses induced by laying vessel motions is based on a profound theoretical investigation of oscillations of slender beams in a fluid excited by arbitrary line forces or motions at the beam's end, published by Weede [18]. The theory is validated by model tests. The associated model testing technique, proposed by Clauss and Kruppa [6] achieves model similarity by defining characteristic numbers derived from the non-dimensional differential equations of pipeline dynamics. Both, the theoretical analysis and the model testing technique have been substantially improved. Calculated and measured motions and stresses of typical pipelines are compared proving the reliability of the proposed method.

Basic Equations

The configuration of the pipeline is defined by the radius vector $\mathbf{r}(s,t)$ of the pipe axis and the torsional angle $\chi(s,t)$ as functions of curve length s and time t, where $()' = \partial/\partial s$ and $(\dot{}) = \partial/\partial t$.

We regard a pipe element with a length of ds. The hydrostatic pressure is acting on the wetted surface. Its resulting force is normal to the pipe axis. It is substituted by a vertical buoyancy force which summons the pressure on the wetted surface and the non-wetted cross sectional areas and - for appropriate correction - axial tension forces which result from the product of the external hydrostatic pressure and the cross sectional areas. The vertical buoyancy contributes to the external line load vector $\mathbf{q}$, and the correcting axial tension forces are added to the internal force vector, i.e. the resultant "effective" force $\mathbf{F}$ consists not only of the stress relevant forces, but also of these axial hydrostatic force corrections.

The basic equations are derived from the dynamic force and moment equilibrium and from the constitutive equations of bending and torsion of circular pipes.

The derivation is shown similar to a flowchart in [18], page 9, and results in a differential equation for the radius vector $\mathbf{r}(s,t)$

$$(EI\mathbf{r}'')''+(EI\kappa^2\mathbf{r}')'-(M_T\mathbf{r}'\times\mathbf{r}'')'-(F_s\mathbf{r}')'+m_0\ddot{\mathbf{r}}=\mathbf{q} \qquad (1)$$

and the well known torsional differential equation

$$(GI_p\chi')' - \Theta\ddot{\chi} = 0$$

The configuration $\mathbf{r}(s,t)$ of the pipe axis is split into a planar static configuration $\mathbf{r}_{st}(s)$ loaded by w, the submerged weight per unit length, and a dynamic deflection $\mathbf{u}(s,t)$ from the vessel motions, waves and current.

The static configuration can be obtained by solving the nonlinear differential equation of the static inclination angle:

$$EI\,\varphi''(s) - H\sin\varphi(s) + (ws - V)\cos\varphi(s) = 0 \qquad (2)$$

In [18], this is derived from Eq. (1), and a very compact analytical approach as well as an efficient and reliable numerical solution is published. The inclination angle $\varphi(s)$ yields the static curvature $|\varphi'(s)|$ for the static bending stresses and the static effective tension force

$$F_{sst}(s) = H\cos\varphi + (ws - V)\sin\varphi \qquad (3)$$

where H is the horizontal force to be decided within the design procedure and V is the bottom support force to be calculated from boundary conditions.

The dynamic configuration is also calculated from Eq. (1) after splitting off the static terms and uncoupling the lateral dynamic component equations (see [18]):

$$EI\,u_N'''' - (F_s u_N')' + m_0\ddot{u}_N = \varphi' F_{sdy} + q_{Ndy} \qquad (4)$$

$$EI\,u_B'''' - (F_s u_B')' + m_0\ddot{u}_B = (\varphi' M_T)' + q_{Bdy} \qquad (5)$$

u_N is the dynamic bending deflection in the static plane and u_B perpendicular to it.

On the left hand side, the dynamic tension force F_{sdy} contributes to the effective tension force $F_s = F_{sst} + F_{sdy}$ introducing a time-dependent stiffness. On the right hand side, it yields a pseudo line load in combination with the static curvature $|\varphi'(s)|$.

As $F_{sdy} = EA\,\epsilon_{dy}$, it depends on the dynamic strain

$$\epsilon_{dy} = u_S' - \varphi' u_N + \frac{u_N'^2}{2} + \frac{u_B'^2}{2} \qquad (6)$$

which is a function of axial motions u_S and lateral motions u_N, u_B.

Axial elastic vibrations are neglected, as the first axial natural frequency is too high to be excited by the seaway. Consequently, the dynamic tension force has nearly the same amplitude and phase all along the pipe and may be averaged over the unsupported span [18,10]:

$$F_{sdy} \approx \frac{1}{L}\int_{(L)} F_{sdy}\, ds \tag{7}$$

The hydrodynamic load components in the unsupported span, q_{Ndy} and q_{Bdy}, are deduced from the generalized Morison equation (see [4]). In the planar case, where the pipe moves with the lateral deflection u, and the external flow velocity from waves and current has the lateral component v, it yields:

$$q_{dy} - m_0\ddot{u} = \underbrace{(1+c_a)\varrho\frac{\pi D^2}{4}\dot{\mathrm{v}} + \underbrace{c_d\frac{\varrho}{2}D|\dot{u}-\mathrm{v}|\,\mathrm{v}}_{b(s,t)} - }_{p(s,t)}$$

$$\underbrace{-(m_0 + c_a\varrho\frac{\pi D^2}{4})\,\ddot{u}}_{m} \underbrace{- c_d\frac{\varrho}{2}D|\dot{u}-\mathrm{v}|\,\dot{u}}_{b(s,t)} \tag{8}$$

where m is the effective mass per unit length, $b(s,t)$ is the damping parameter and $p(s,t)$ is the load contribution from waves and current.

Beyond the touch down point, the pipe on the sea floor is treated as a generalized Winkler beam with linear elasticity, damping and inertia forces. k is the beam subgrade modulus, b expresses soil damping, and m includes soil added mass.

The dynamic problem can be summarized as follows:

$$EIu_N'''' + (F_s u_N')' + ku_N + m\ddot{u}_N + b\dot{u}_N = \varphi' F_{sdy} + p_N \tag{9}$$

$$EIu_B'''' + (F_s u_B')' + ku_B + m\ddot{u}_B + b\dot{u}_B = (\varphi' M_T)' + p_B \tag{10}$$

$$F_{sdy} = \frac{EA}{L}\left[u_{sL} - \int_{(L)}\left(\varphi' u_N - \frac{u_N'^2}{2} - \frac{u_B'^2}{2}\right) ds\right] \tag{11}$$

parameters in the unsupported span ($s > 0$):

$$k = 0 \qquad m = m_0 + c_a\varrho\frac{\pi D^2}{4}$$

$$b = c_d\frac{\varrho}{2}D\sqrt{(\dot{u}_N - \mathrm{v}_N)^2 + (\dot{u}_B - \mathrm{v}_B)^2}$$

$$p_N = (1+c_a)\varrho\frac{\pi D^2}{4}\dot{\mathrm{v}}_N + b\mathrm{v}_N \qquad p_B = (1+c_a)\varrho\frac{\pi D^2}{4}\dot{\mathrm{v}}_B + b\mathrm{v}_B$$

parameters on the seabed ($s < 0$):
$p_N = p_B = 0$ and k, m, b from linearized soil mechanics

If the tensioner is compensating, i.e. $F_{sdy} = 0$, Eq. (11) has to be resolved with respect to the boundary axial motion $u_{sL}(t)$. The difference between $u_{sL}(t)$ and the vessel's axial motion component ist the relative axial motion between vessel and pipe. If the tensioner is blocked, $u_{sL}(t)$ is the vessel's axial motion component and Eq. (11) is coupled with Eqs. (9) and (10).

Linearized Dynamic Solution

The dynamic deflections and the corresponding dynamic tension force are calculated from Eqs. (9)-(11). Linearization consists of three assumptions: The total effective tension force $F_s(s,t)$ on the left hand side of Eqs. (9) and (10) is approximated by its static value $F_{sst}(s)$; the square strain terms in Eq. (11) are neglected; for the hydrodynamic damping parameter $b(s,t)$ a time independent approximation $\tilde{b}(s)$ is taken and improved iteratively to minimize the square error of the drag force.

After introducing these assumptions, Eqs. (9), (10) and (11) as well as the dynamic boundary conditions, i.e. the vessel motions, are converted to frequency domain using the general definitions

$$f(t) = \sum_{j=-n}^{n} f_j\, e^{i\omega_j t} \qquad f_j = \frac{1}{T}\int_{(T)} f(t)\, e^{-i\omega_j t}\, dt$$

where f_j are the complex Fourier coefficients and $\omega_j = j \cdot 2\pi/T$ are the circular frequencies with T being a sufficiently large time window.

As the right hand side of Eq. (9) contains the dynamic tension force F_{sdy}, which is unknown unless the tensioner compensates, the Fourier transform of Eq. (9) cannot be solved directly.

Introducing

$$u_{Nj} = u_{Nj}^{(0)} + F_{sj}u_{Nj}^{(1)} \tag{12}$$

the Fourier transform of Eq. (9) is split into two equations for $u_{Nj}^{(0)}$ and $u_{Nj}^{(1)}$ whose right hand sides are known; $u_{Nj}^{(0)}$ is the contribution from vessel motions, waves and current and has to be calculated with inhomogenuous boundary conditions from the vessel motions, and $u_{Nj}^{(1)}$ is the contribution from the dynamic tension force and has to be calculated with homogenuous boundary conditions (all boundary values being zero).

To obtain the complex Fourier coefficients F_{sj} of the dynamic tension force if the tensioner is blocked, Eq. (12) is introduced into the Fourier transform of Eq. (11) neglecting the square terms:

$$F_{sj} = \frac{EA}{L}\left[u_{sLj} - \int_{(L)}\varphi'\left(u_{Nj}^{(0)} + F_{sj}u_{Nj}^{(1)}\right) ds\right]$$

and this is resolved with respect to F_{sj}.

The linear solution is summarized as follows:
Differential equations (see [18] for numerical solution):

$$EIu_{Nj}^{(0)\prime\prime\prime\prime} - (F_{sst}u_{Nj}^{(0)\prime})' + (k - \omega_j^2 m + i\omega_j\tilde{b})u_{Nj}^{(0)} = p_{Nj} \tag{13}$$

with inhomogenuous boundary conditions from vessel motions

only if the tensioner is blocked:

$$EIu_{Nj}^{(1)\prime\prime\prime\prime} - (F_{sst}u_{Nj}^{(1)\prime})' + (k - \omega_j^2 m + i\omega_j\tilde{b})u_{Nj}^{(1)} = \varphi' \tag{14}$$

with homogenuous boundary conditions: all zero

$$EIu_{Bj}'''' - (F_{sst}u_{Bj}')' + (k - \omega_j^2 m + i\omega_j\tilde{b})u_{Bj} = (\varphi' M_{Tj})' + p_{Bj} \tag{15}$$

with inhomogenuous boundary conditions from vessel motions

Composition:

blocked tensioner	compensating tensioner
$F_{sj} = \dfrac{u_{sLj} - \int_{(L)} \varphi' u_{Nj}^{(0)}\, ds}{\dfrac{L}{EA} + \int_{(L)} \varphi' u_{Nj}^{(1)}\, ds}$ (16)	$u_{sLj} = \int_{(L)} \varphi' u_{Nj}^{(0)}\, ds$ (17)
$u_{Nj} = u_{Nj}^{(0)} + F_{sj}\, u_{Nj}^{(1)}$	$u_{Nj} = u_{Nj}^{(0)}$

The numerical solution is embedded in two nested loops. The internal loop steps along the circular frequencies $\omega_j = j \cdot 2\pi/T$, $j = 0,1,2,\ldots$. The external loop serves to improve the linearized damping parameter:

$$\tilde{b}(s) = c_d \frac{\varrho}{2} D \frac{\int_{(T)} \left[(\dot{u}_N - v_N)^2 + (\dot{u}_B - v_B)^2\right]^{3/2} dt}{\int_{(T)} \left[(\dot{u}_N - v_N)^2 + (\dot{u}_B - v_B)^2\right] dt} \qquad (18)$$

Nonlinear Dynamic Correction

The bending deflections and the parameters are split into a linear and a nonlinear part:

total = linear + nonlinear
$u_N(s,t) = u_{0N}(s,t) + u_{1N}(s,t)$
$u_B(s,t) = u_{0B}(s,t) + u_{1B}(s,t)$
$F_{sdy}(t) = F_0(t) + F_1(t)$
$b(s,t) = \tilde{b}(s) + \Delta b(s,t)$

The unknown nonlinear correction is modally decomposed:

$$u_{1N} = \sum_{(j)} u_j(s)\tau_{Nj}(t) \qquad u_{1B} = \sum_{(j)} u_j(s)\tau_{Bj}(t)$$

where $u_j(s) = j$th normalized mode shape and $\Omega_j = j$th natural circular frequency.
All other functions of s are modally decomposed, following the general definition

$$f(s) = \sum_{(j)} u_j(s) f_j \quad \text{where } f_j = \int_{(L)} f(s) u_j(s)\, ds$$

After splitting off the known linear solution from Eqs. (9) and (10) and introducing these modal decompositions, the nonlinear part of Eqs. (9) and (10) yields two systems of differential equations for the $\tau_{Nj}(t)$ and $\tau_{Bj}(t)$ which can be uncoupled as follows:

$$m\ddot{\tau}_{Nj} + \beta_{jj}\dot{\tau}_{Nj} + (\Omega_j^2 m + F_{sdy} c_{jj})\tau_{Nj} = \\ = -F_{sdy} c_{jj} T_{Nj} - \Delta\beta_{jj}\dot{T}_{Nj} + F_1 \kappa_j \qquad (19)$$

$$m\ddot{\tau}_{Bj} + \beta_{jj}\dot{\tau}_{Bj} + (\Omega_j^2 m + F_{sdy} c_{jj})\tau_{Bj} = \\ = -F_{sdy} c_{jj} T_{Bj} - \Delta\beta_{jj}\dot{T}_{Bj} \qquad (20)$$

The magnitudes $\beta_{jj}, \Delta\beta_{jj}, c_{jj}, \kappa_j$ from the parameters and T_{Nj}, T_{Bj} from the linear solution are explained in the list of symbols.
These two uncoupled equation systems (19) and (20) are solved with the Newmark method [3]. Their parameter $F_{sdy}(t)$ is zero if the tensioner is compensating and unknown if it is blocked.

For the case of blocked tensioner an expression for the relative axial deflection $\Delta u_s(t)$ between pipe and vessel was developed from Eq. (11), and at each timestep a binary search takes place to find the F_{sdy} which makes Δu_s to zero.
Using the known linear part F_0 of F_{sdy} and the above modal decompositions, this relative axial deflection is

$$\Delta u_s = \frac{L}{EA}(F_{sdy} - F_0) + \\ + \sum_{(j)} \left[\kappa_j \tau_{Nj} - \frac{c_{jj}}{2}(T_{Nj} + \tau_{Nj})^2 - \frac{c_{jj}}{2}(T_{Bj} + \tau_{Bj})^2\right] \qquad (21)$$

Note that the τ_{Nj}, τ_{Bj} mutually depend on F_{sdy}. For a detailed description of the procedure see [18].

Model Tests and Validation

The calculation methods are validated with model tests. To ensure a realistic range of parameters, the model tests maintain model similarity to typical full scale examples.
The basic equations and their boundary conditions are transformed into a non-dimensional form. As any mechanical dimension can be composed of length, force and time, lengths are normalized by the characteristic length H/w, forces are normalized by the characteristic force H and times are normalized by the characteristic time $\sqrt{mH}/\mathrm{w}$. The parameters of the non-dimensional formulation, as far as their influence can't be neglected, are the characteristic numbers. The model test is mechanically similar to a specific full scale problem if the characteristic numbers have the same values in model scale as in full scale.
The three most crucial characteristic numbers are

$\frac{\mathrm{w}d}{H}$ = non-dimensional depth
$\frac{EI\mathrm{w}^2}{H^3}$ = non-dimensional flexural rigidity
$\frac{\omega\sqrt{mH}}{\mathrm{w}}$ = non-dimensional frequency

A different set of characteristic length, force and time yields a different, but equivalent set of characteristic numbers [6].
Model magnitudes are now marked with an asterisk ()*. To simulate different full scale examples with the same model pipeline, the three most crucial characteristic numbers are adjusted by three magnitudes which can easily be varied previously to every model test: the horizontal force H^*, the lay depth d^* and the circular frequency ω^* of the sinusoidal excitation. The above expressions for the three characteristic numbers are equated for full scale and model scale; these three coupled equations are resolved with respect to H^*, d^* and ω^*.
This yields the scales of the three basic dimensions:

$$\text{length scale} = \lambda_l = \frac{d}{d^*} = \left(\frac{EI\mathrm{w}^*}{(EI)^*\mathrm{w}}\right)^{1/3}$$

$$\text{force scale} = \lambda_f = \frac{H}{H^*} = \left(\frac{EI\mathrm{w}^2}{(EI)^*\mathrm{w}^{*2}}\right)^{1/3}$$

$$\text{time scale} = \lambda_t = \frac{T}{T^*} = \frac{\omega^*}{\omega} = \\ = \left(\frac{m}{m^*}\right)^{1/2} \left(\frac{EI}{(EI)^*}\right)^{1/6} \left(\frac{\mathrm{w}^*}{\mathrm{w}}\right)^{2/3} = \left(\frac{m}{m^*}\frac{\lambda_l^2}{\lambda_f}\right)^{1/2}$$

As a fourth characteristic number the non-dimensional damping parameter $c_d \frac{\varrho}{2} D \frac{H}{\mathrm{w}m}$ is kept close to the full scale values by dimensioning the model pipeline.

Two typical examples were used for experimental validation:

location	Frigg-Karmøy	Strait of Messina
see literature	[14]	[16]
steel pipe ext.diameter	406 mm	508 mm
steel wall thickness	15.9 mm	23.8 mm
concrete coating thickness	63.5 mm	0 mm
subm. weight per length w	1215.7 N/m	843.66 N/m
eff. mass per length m	582 kg/m	501.50 kg/m
flexural rigidity EI	76.7 MNm^2	219.09 MNm^2
laying depth d	150 m	237 m
horizontal force H	333 kN	279 kN
length scale λ_l	43.477	69.597
force scale λ_f	14827	16471
time scale λ_t	6.458	9.110

The model pipeline (Fig. 2) consists of two components. A rectangular stainless steel strip contributes $(EI)^*$, most of w* and part of m^*. It is surrounded by segments of perspex pipe which contribute the other part of m^* (including the trapped water), D^* and the small remainder of w*. The pipe is segmented to avoid an influence on EI^*. This allows to dimension both components rather independently from each other in order to suit the model pipeline to the requirements of model similarity. For stress measurements, the steel profile is equipped with strain gauges in distances of about 60 cm.

Model pipeline specifications:

width of steel strip		= 20 mm
thickness of steel strip		= 2 mm
external diameter of segments	D^*	= 30 mm
wall thickness of segments		= 3 mm
submerged weight per unit length	w*	=3.5646 N/m
effective mass per unit length	m^*	=1.7771 kg/m
flexural rigidity	$(EI)^*$	=2.7467 Nm^2

The experiments are carried out in a deep water tank with a length of 12 m, a width of 1.3 m and a depth of about 5 m. At one side, the tank is equipped with windows.

All equipment is installed in a large steel frame which is movable around a bearing at the top end of the tank (Fig. 2). It can be lifted with an electrical crane to access it above the water surface.

To simulate the laying vessel motions in the seaway, the upper end of the pipeline is hinged to a planar motion mechanism. This mechanism provides a unidirectional harmonic oscillation whose direction, amplitude and frequency can be varied arbitrarily. It is equipped with a directional load cell whose two signals can be geometrically transformed into tension and sheer force.

At the opposite end, the pipeline lays on a model "seabed", which can be fixed horizontally at different depths d^* below the upper end. To simulate soil elasticity, this soil model consists of a series of U-shaped steel elements which are bridged with a tensioned steel wire. The pipe, after touch-down, is supported by these steel wires, their tension being adjusted with screws to represent a defined subgrade modulus. A series of such bottom supports are positioned at distances of 20 cm. At the very end of this soil model, the pipe is attached to a load cell. Its position can be shifted horizontally to adjust the static horizontal force.

The dynamic response is investigated with two methods:

- long time photographs of small diodes attached to the pipeline to register trajectories
- computer based registration of time series from:
  - strain gauges located along the pipeline,
  - the load cell at the bottom
  - the directional load cell at the top

The trajectory photographs are compared with the theory by linking the theoretical subroutines to a main program which draws trajectories in exactly the same scale. These results are presented in Fig. 3, modelling the Messina pipeline.

In Fig. 4, the computer registered time series are evaluated, modelling the Frigg-Karmøy pipeline. They are accompanied by a theoretical simulation of each model test. The calculated time series are transformed into A/D converter units and written to a file in exactly the same format as the measured data. This allows to process both measured and calculated data with the same software. At each individual timestep the dynamic bending stresses are interpolated between the strain gauges with the parabolic blending method and drawn as stress distribution along the pipeline. Fig. 4 shows these results comparing model tests (right) and theory (left) at different frequencies from a slow variation of the static configuration (top) up to a fast motion (bottom). The shape of the stress curves at the lowest frequency (upper diagrams) has one node erroneously suggesting the second mode shape. However, this variation of the stress along the pipeline results from the varying positions of the hinged upper end of the pipeline and the associated steady-state pipe geometries. At higher frequencies, the number of nodes increases, and the dynamic response is distorted by the nonlinear interaction with the dynamic tension force and by the hydrodynamic damping.

The calculated stresses compare well with the measured ones. Only one of the measured strain gauge signals differs remarkably from the theory. This strain gauge, located near the touch down point, was checked and found to work unreliably.

The upper and lower pair of stress diagrams is accompanied by time series of the dynamic tension forces. They clearly prove the nonlinear behaviour. For confirming the hypothesis that the dynamic tension force does not depend on the curve length s (Kirchhoff's hypothesis [10]), it is measured at both ends of the pipeline. The corresponding two diagrams on the right side show that both load cell signals, indeed, are equal.

Full Scale Examples

Finally, full scale calculations have been performed taking the Strait-of-Messina pipeline as an example (see above).

The dynamic tension forces in a suspended pipe due to motions of the stinger and layvessel could become very large if the pipe is held fixed relative to the vessel. To damp out these potentially large tension oscillations, tension machines designed for deepwater will have to "give", thus permitting small axial motions of the pipe whenever the tension passes outside a specified "deadband" range which, for example, may be ±10 % of the static tension. However, when the dynamic loads fall within the deadband range, the pipe must be held rigidly to the vessel, except during pipe payout, as this allows pipe fabrication operations to progress at a maximum rate [13].

The following examples, shown in Figs. 5-7, illustrate the two limiting cases

- blocked tensioner: no axial motions, high axial forces due to the vessel motions (left side of each figure)
- compensating tensioner: no axial forces, significant axial motions due to the relative movements between pipehead and vessel (right side of each figure).

In practice, both modes are relevant during laying operations, as an upper tension limit is dictated by tensioner capacity and a lower limit by static considerations.

The figures illustrate how the dynamic response to a planar harmonical vessel motion depends on various operational parameters. Varying one parameter, four pairs of diagrams are presented. The left diagram of each pair shows the pipe motions and - alphanumerically - the varied parameter as well as the range of the dynamic part of the tension force (blocked tensioner) or of the axial motions of the pipe head (compensating tensioner). The right diagram of each pair shows the corresponding total stress distribution along the upper and the lower fiber of the pipe as two static curves surrounded by their dynamic envelopes.

In Fig. 5, the period T of a lateral excitation with an amplitude of 1 m has been varied. The dynamic stresses increase with the frequency. Evidently, this behaviour depends on the ratio of the excitation frequency to the first natural frequency. As a consequence a stiff system helps to reduce the dynamic stress envelope.

Fig. 6 demonstrates that maximum dynamic stress envelopes occur in shallow water. The lay depth d has been varied, investigating a lateral excitation with an amplitude of 1 m and a period of 4 s.

For the same excitation, Fig. 7 shows a variation of the horizontal force H. Increasing the tension force seems to reduce the dynamic envelopes. Investigations have shown, however, that in other cases the opposite influence may occur. H has to be decided upon at the design state. This figure demonstrates that mainly the static stresses, not the dynamic envelopes, are relevant for this decision.

All these examples are focussed on the excitation component lateral to the pipe. Fig. 8 illustrates the effect of other directions of excitation with a period of 4 s and 8 s and an amplitude of 1 m. With a blocked tensioner, the dynamic stress and motion envelopes as well as the dynamic tension force amplitudes have their maximum at axial excitation. In many cases, as has been proved for a variety of calculations of other pipelines and operational parameters, axial excitation yields tension force amplitudes far beyond any tensioner capacity if the tensioner is blocked. Needless to say that the tensioner will ease off if overloaded.

Comparing the two alternatives of blocked or compensating tensioner it is evident that any pipe laying procedure has to cope with high alternating axial tension forces or relative motions between pipe and tensioner.

- Alternating axial tension forces are limited by the tensioner design capacity. Thus, the related stress variations are just illustrating the adverse effects of tensioner blockage.
- In the second case of a tensioner pulling with a defined constant force, the pipeline experiences relative motions which are resulting from the pipe motions at top superimposed by the vessel motions with respect to phase.

In both cases, favorable motion characteristics are advantageous which explains the preference for semisubmersible laying vessels.

Conclusions

The paper presents a unique theory for calculating dynamic motions and stresses of pipelines during laying operations. Special attention is given to the nonlinear interaction between bending oscillations and dynamic tension as well as to linearized pipe-soil interaction.

The calculation methods have been successfully validated with model tests. The model tests have been carried out with a sophisticated technique, yielding dynamic stress distributions, dynamic tension forces and trajectory photographs. They are performed within a realistic range of parameters, based on the special model similarity laws of a bending beam oscillating in water. It has been pointed out that dynamic effects pose severe problems at rough sea conditions, especially if the laying vessel responds to short waves with high amplitudes. A stiff system, i.e. a high first natural frequency, helps to reduce the dynamic response by keeping the excitation frequencies low in comparison to the natural frequencies. This should be taken into account when deciding upon the horizontal force H.

Blocking of the tensioner results in extremly high axial dynamic forces which may overload the tensioner. Operating the tensioner with constant tension force is associated with axial motions between laying vessel and pipeline which has to be considered in designing the manufacturing procedure. Thus a sophisticated tensioner operation is recommended.

Sample calculations prove that dynamic effects are significant at any laying operation. The theoretical method is versatile and allows for adaption to any specific laying problem.

List of Symbols

$b(s,t)$	=	damping parameter; in the unsupported span: $b = \frac{1}{2} c_d \varrho D \sqrt{(\dot{u}_N - v_N)^2 + (\dot{u}_B - v_B)^2}$
$\tilde{b}(s)$	=	linearized damping parameter
c_a, c_d	=	Morison's added mass and drag coefficient
c_{jj}	=	square of the 1st derivative of the j-th normalized mode shape, integrated over the unsupported length
D	=	largest diameter, diameter of concrete hull
d	=	vertical distance from seabed to top of stinger circle (S-method) or to the clamped end (J-method)
EA	=	axial rigidity of steel pipe
EI	=	flexural rigidity of steel pipe
$F_s(s,t)$	=	effective tension force = real tension force + displacing cross sectional area times external hydrostatic pressure
$F_{sst}(s)$	=	static part of effective tension force
$F_{sdy}(t)$	=	dynamic part of effective or real tension force
F_{sj}	=	j-th complex Fourier coefficient of the linearized dynamic tension force $F_0(t)$
$F_0(t)$	=	linear part of dynamic tension force $F_{sdy}(t)$
$F_1(t)$	=	nonlinear part of dynamic tension force $F_{sdy}(t)$
H	=	static horizontal force
k	=	on the soil: beam subgrade modulus; in the unsupported span: zero
L	=	unsupported length
$M_T(s,t)$	=	torque or torsional moment
$M_{Tj}(s)$	=	j-th complex Fourier coefficient of M_T
m	=	effective mass per length of pipe incl. hydrodynamic mass (on the soil plus subgrade added mass)
m_0	=	mass per length of the pipe only
$p_N(s,t)$	=	$(1+c_a)\varrho\frac{1}{4}\pi D^2 \dot{v}_N + b v_N$ = wave and current contribution to the lateral hydrodynamic line load in the static plane (N)

$p_B(s,t)$ = $(1+c_a)\varrho\frac{1}{4}\pi D^2\dot{v}_B + bv_B$ = wave and current contribution to the lateral hydrodynamic line load perpendicular to the static plane (B)

$p_{Nj}(s), p_{Bj}(s)$= j-th complex Fourier coefficient of p_N, p_B

$q(s,t)$ = generally: line load vector

$q_{Ndy}(s,t), q_{Bdy}(s,t)$= lateral dynamic line loads in the static plane (N) and perpendicular to it (B).

$r(s,t)$ = radius vector of pipe axis from static touch down point; static part r_{st}, dynamic part u

s = curve length from static touch down point, upwards positive

$T_{Nj}(t), T_{Bj}(t)$= j-th modal coefficient of the linearized bending deflections u_{0N}, u_{0B}, i.e. their product with the j-th mode shape integrated over the unsupported span.

t = time

$u_j(s)$ = j-th normalized mode shape

$u_N(s,t), u_B(s,t)$= dynamic bending deflections in the static plane (N) and perpendicular to it (B)

$u_{Nj}(s), u_{Bj}(s)$= j-th complex Fourier coefficient of the linearized bending deflections u_{0N}, u_{0B}

$u_{Nj}^{(0)}(s)$ = contribution to u_{Nj} from lateral loads and boundary conditions; see $u_{Nj} = u_{Nj}^{(0)} + F_{sj}u_{Nj}^{(1)}$

$u_{Nj}^{(1)}(s)$ = contribution to u_{Nj} from dynamic tension force; see $u_{Nj} = u_{Nj}^{(0)} + F_{sj}u_{Nj}^{(1)}$

$u_S(s,t)$ = axial dynamic deflection

$u_{SL}(t)$ = boundary value of u_S at upper end of unsupported span

Δu_s = axial relative motion = u_{SL} minus axial component of vessel motion

$u_{0N}(s,t), u_{0B}(s,t)$= linear part of the dynamic bending deflections u_N, u_B

$u_{1N}(s,t), u_{1B}(s,t)$= nonlinear linear part of the dynamic bending deflections u_N, u_B

$v_N(s,t), v_B(s,t)$= lateral components of the external flow velocity in the static plane (N) and perpendicular to it (B).

w = submerged weight per length (weight in air minus buoyancy)

β_{jj} = damping parameter by sqare of j-th normalized mode shape, integrated over the unsupported lenght

$\Delta\beta_{jj}$ = nonlinear part of β_{jj}

$\epsilon_{dy}(s,t)$ = dynamic part of the strain of the pipe axis

$\kappa(s,t)$ = $|r''|$ = curvature of pipe axis

κ_j = j-th modal coefficient of $\varphi'(s)$

ϱ = specific mass of sea water = $1025\ kg/m^3$

$\tau_{Nj}(t), \tau_{Bj}$ = j-th modal coefficient of the nonlinear part u_{1N}, u_{1B} of the bending deflection

$\varphi(s)$ = static inclination angle

$|\varphi'(s)|$ = static curvature

Ω_j = j-th natural circular frequency

ω_j = $j \cdot \Delta\omega$ = j-th discrete circular frequency

References

[1] Bliek, A.;Triantafillou, M.S.: Nonlinear Cable Dynamics. Behaviour of Offshore Structures, Elsevier Science Publishers B.V., Amsterdam 1985, pp.963-972

[2] Borgman,L.E.: Ocean wave simulation for engineering design. Journal of the Waterways and Harbors Division, ASCE 1969, 95 (WW4), pp.557-583

[3] Burnett, D.S.: Finite Element Analysis. Addison-Wesley Publishing Company, Reading 1987

[4] Clauss,G.F.;Lehmann,E.;Östergaard,C.: Meerestechnische Konstruktionen. Springer-Verlag, Berlin 1988

[5] Clauss,G.;Kruppa,C.;Wolf,E.;Stamm,K.: Parameterstudie über das Verlegen von Pipelines in großen Meerestiefen. Meerestechnik 8 (1977) Nr.3 Juni, pp. 83-88

[6] Clauss,G.;Kruppa,C.: Model Testing Techniques in Offshore Pipelining. OTC 1937, Houston 1974

[7] Clauss,G.F.; Weede,H.E.W.: Dynamics of pipelines during laying operations. Offshore Engineering. Proc.7th Int.Symp.on Offsh.Eng. held at COPPE, Fed.Univ. of R.J., Brazil, Aug.1989. Pentech Press, London 1990

[8] Gardner,T.N.; Kotch,M.A.: Dynamic Analysis of Risers and Caissons by the Element Method. OTC 2651, Houston 1976

[9] Hapel,K.;Köhl,M.: Erzwungene Transversalschwingungen langer Drilling-Riser - der Dämpfungsparameter der linearisierten Widerstandskraft. Der Stahlbau 11 (1980), pp. 335-384

[10] Kauderer,H.: Nichtlineare Mechanik. Springer-Verlag Berlin/Göttingen/Heidelberg 1958, p. 658

[11] Kirk,C.L.;Etok,E.U.: Wave Induced Random Oscillations of Pipelines During Laying. Applied Ocean Research, 1979, Vol.1, No.1, pp. 51-60

[12] Krolikowski,L.P.; Gay,T.A.: An improved linearization technique for frequency domain riser analysis. OTC 3777, Houston 1980

[13] Langner,C.G.;Ayers,R.R.: The Feasibility of laying Pipelines in deep Waters. OMAE 85, Houston 1985, pp.478-489

[14] Lund,S.: Geplante Pipeline durch den Norwegischen Graben. Meerestechnik mt 7 (1976) Nr.5, Oktober. pp.165-172

[15] Malahy,R.C.: A Nonlinear Finite Element Method for the Analysis of Offshore Pipelines, Risers and Cable Structures. Proceedings of the 5th OMAE Symposium, Tokyo 1986, pp. 471-478

[16] Pipes & Pipelines International, Dec.79, p.18

[17] Vlahopoulos,N.;Bernitsas,M.: Three-dimensional nonlinear analysis of pipelaying. Applied Ocean Research 1990, Vol.12, No.3, pp.112-125

[18] Weede,H.: Dynamik offshoretechnischer Linientragwerke am Beispiel der Pipelineverlegung. Dissertation, TU Berlin, 1990

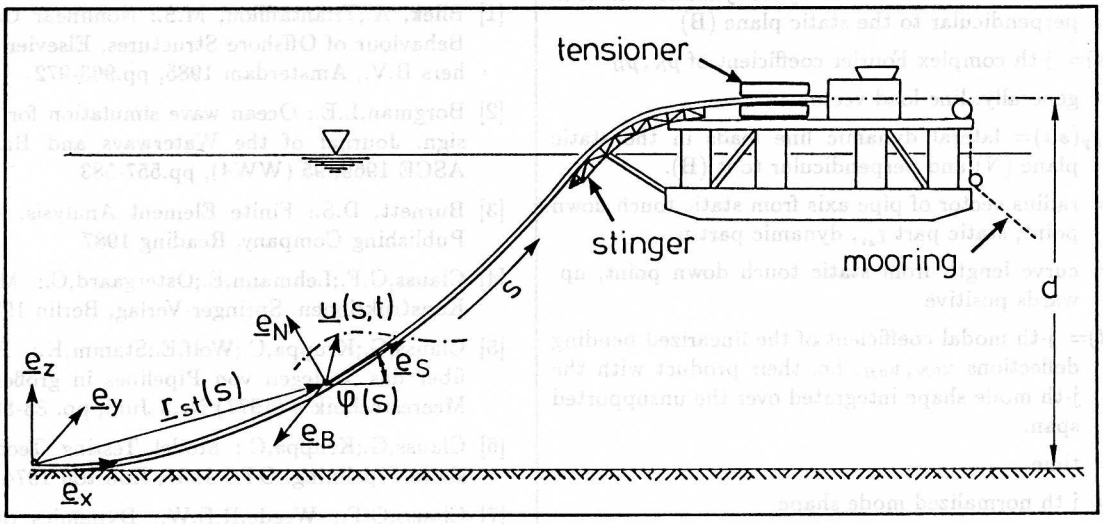

Fig.1 Principle of offshore pipelaying (S-method)

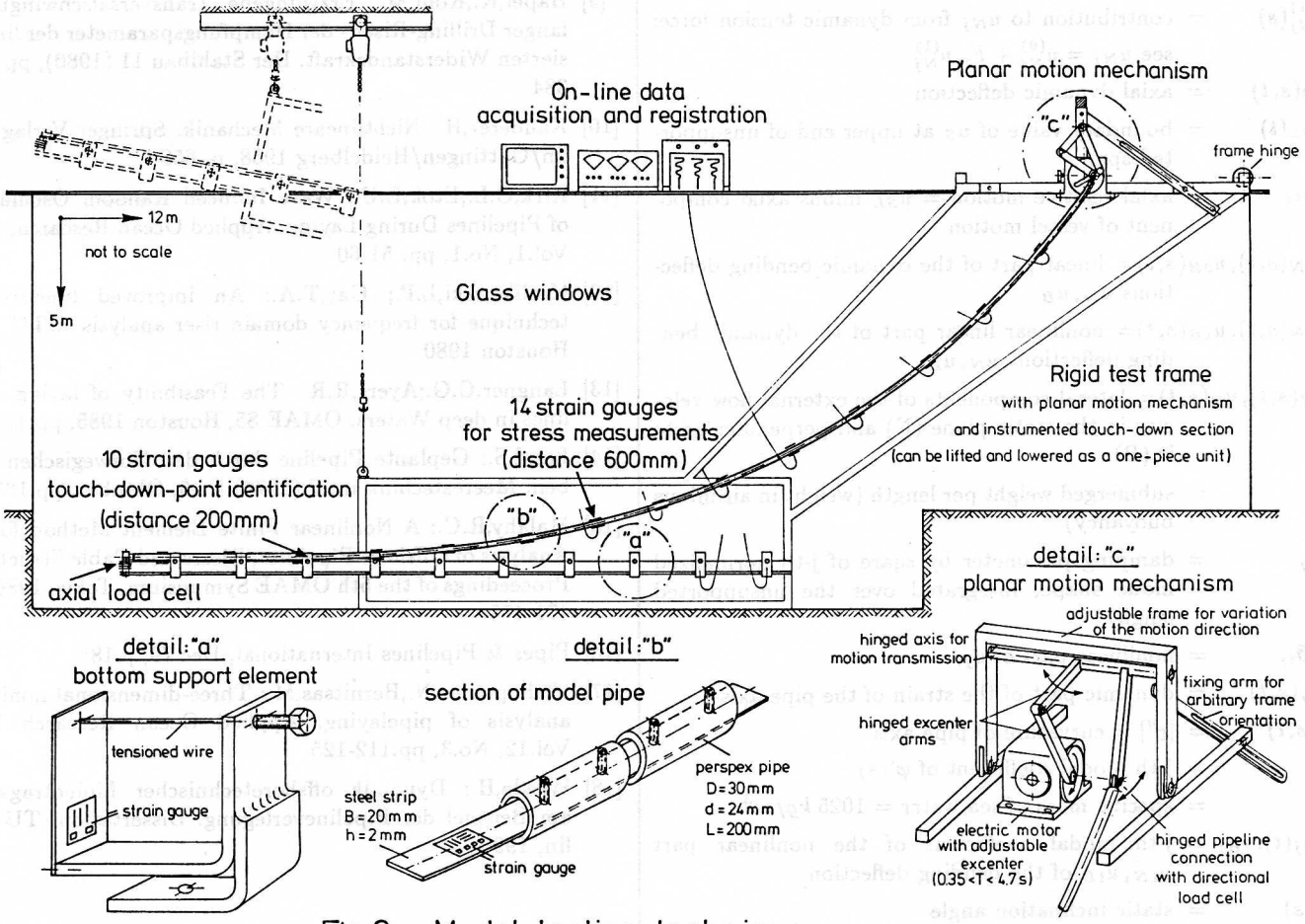

Fig.2 Model testing technique

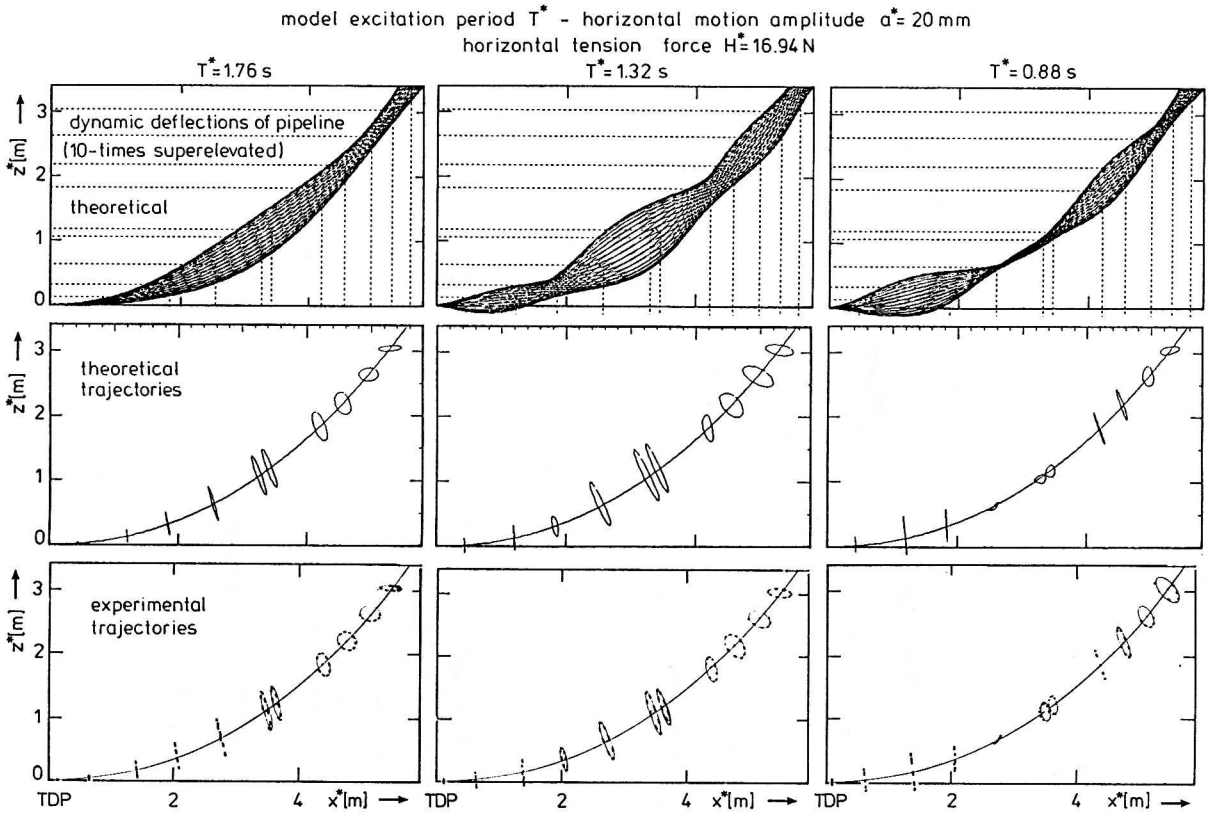

Fig.3 Pipeline dynamics-comparison of theoretical and experimental trajectories (horizontal excitation)

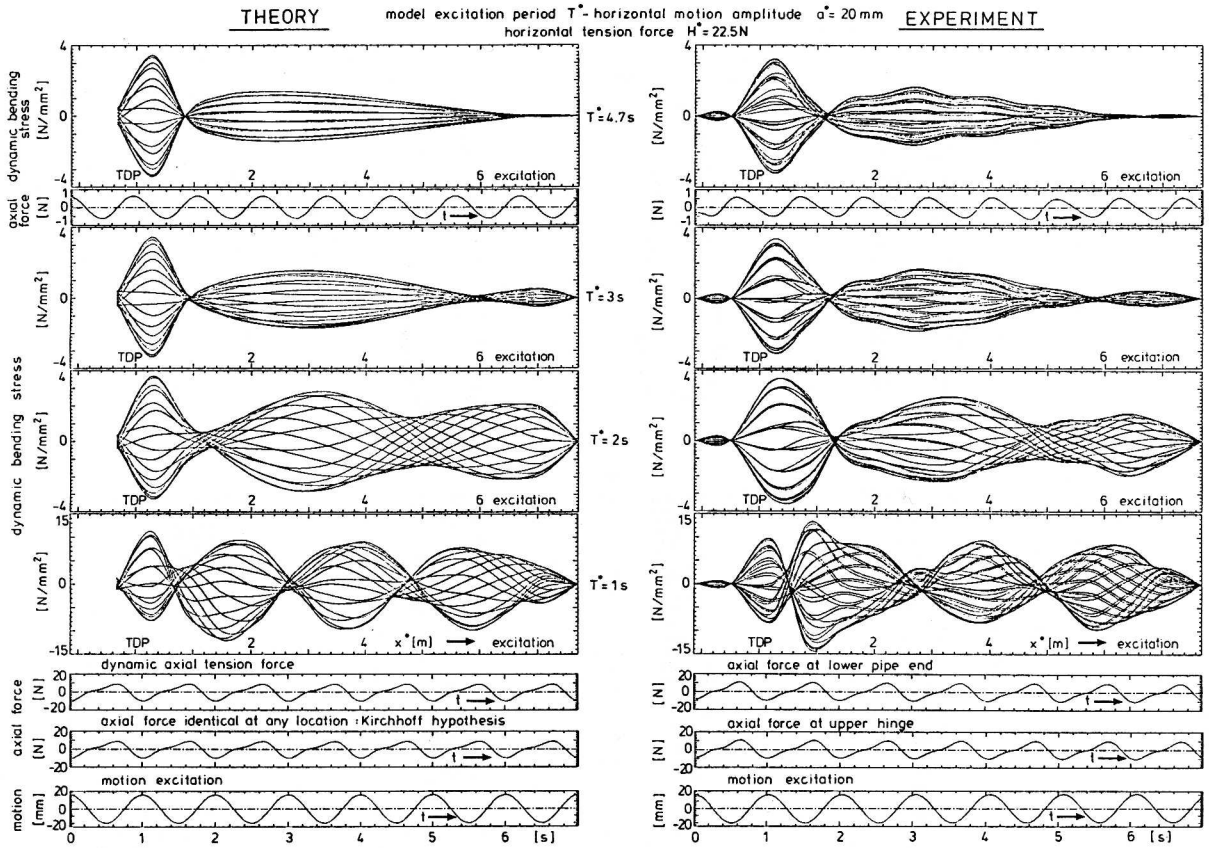

Fig.4 Pipeline dynamics-comparison of theoretical and experimental stresses and forces

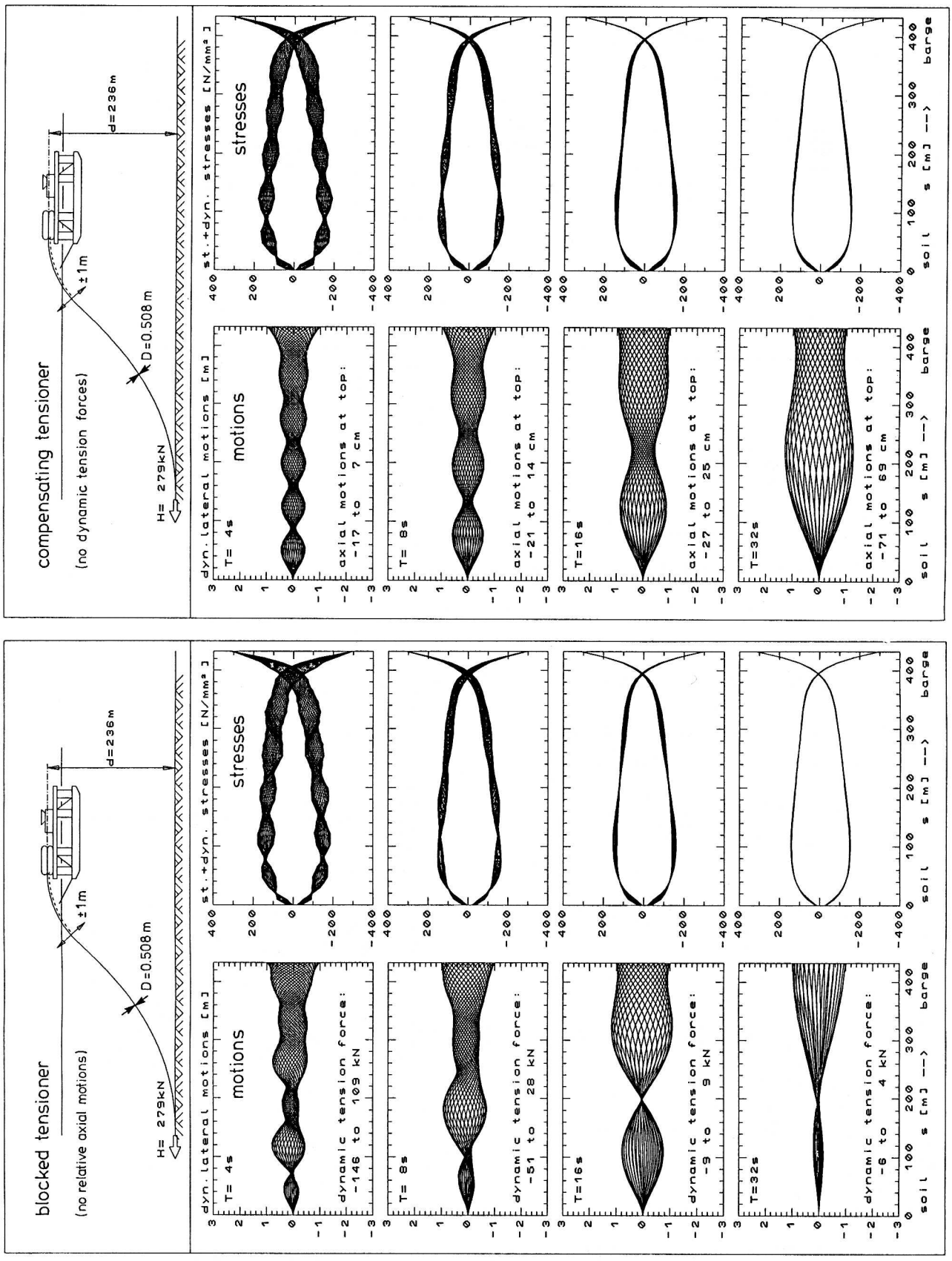

Fig. 5 Dynamics of offshore pipelines during laying - variation of motion (wave) period T (lateral excitation)

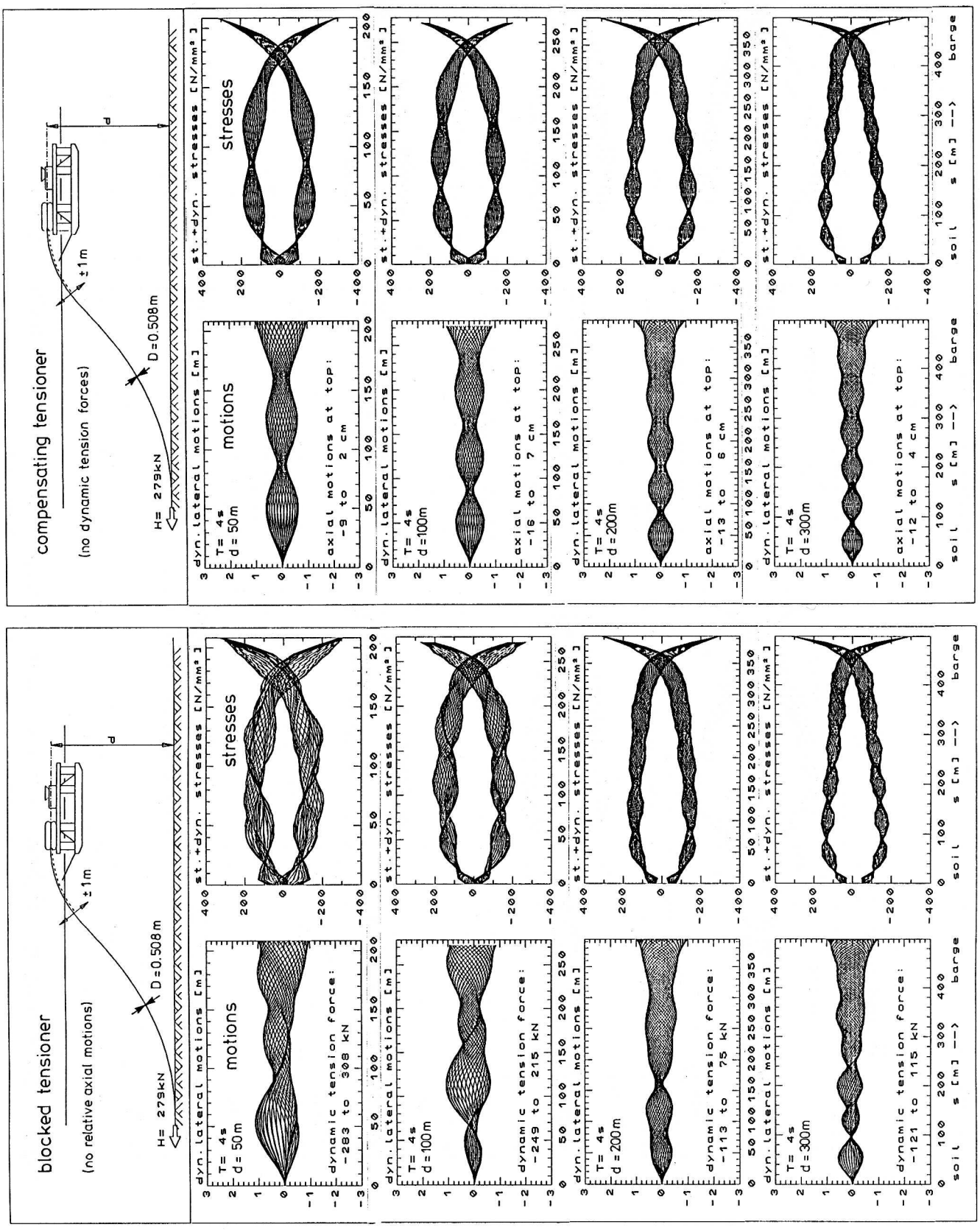

Fig. 6 Dynamics of offshore pipelines during laying - variation of water depth (lateral excitation)

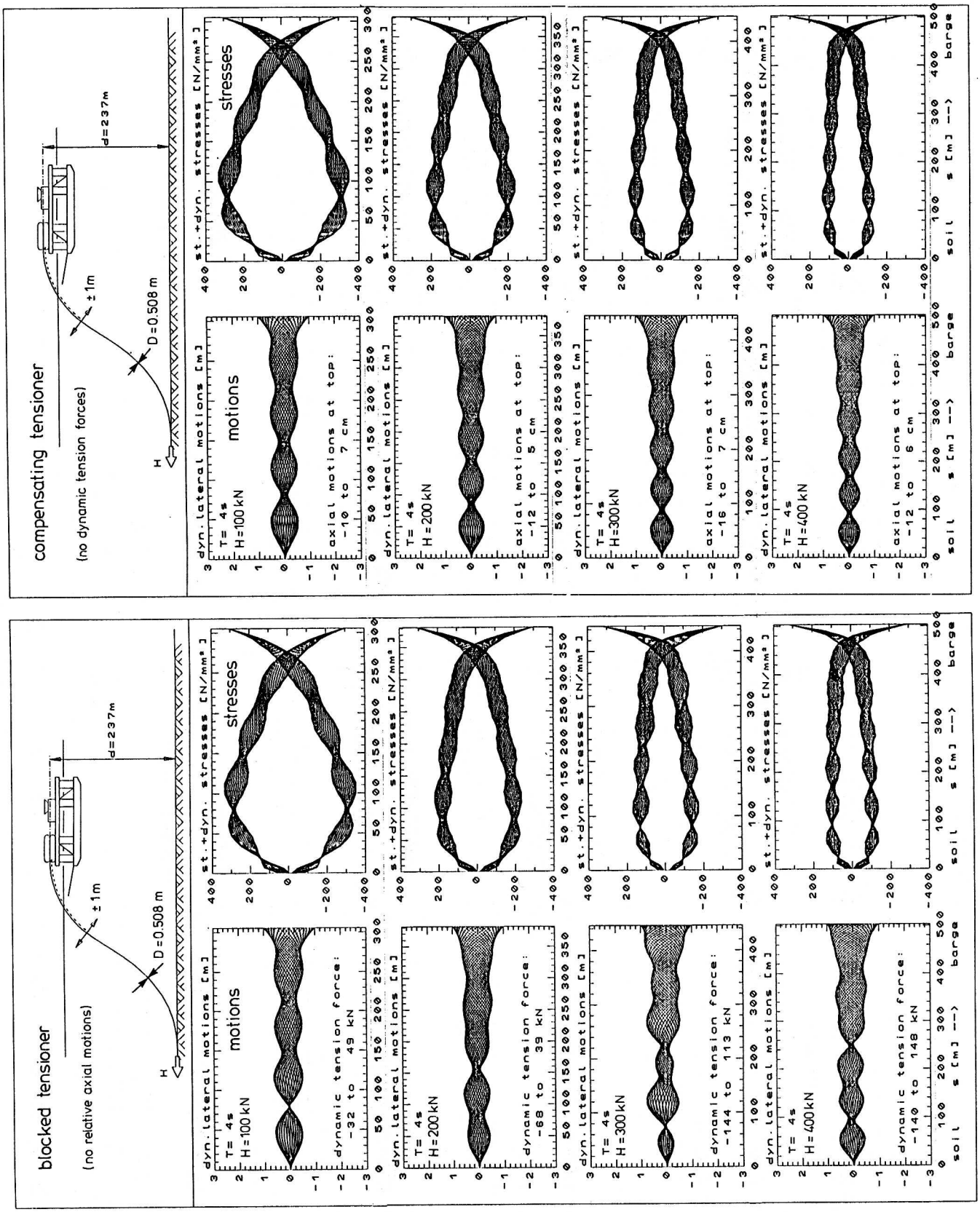

Fig. 7 Dynamics of offshore pipelines during laying - variation of tension force (lateral excitation)

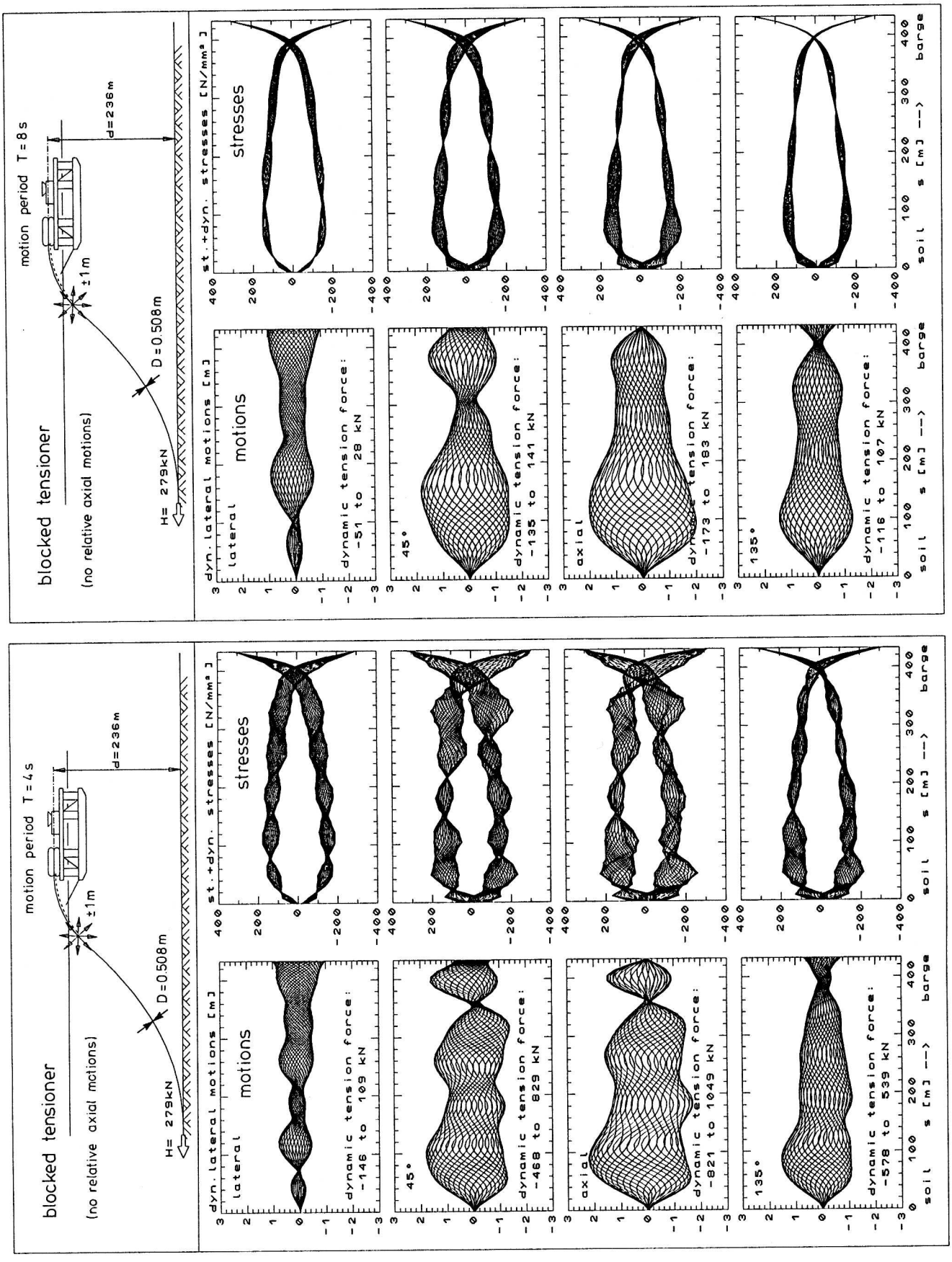

Fig. 8 Dynamics of offshore pipelines during laying - variation of excitation direction